Analytical spectral design of mechanical metamaterials with inertia amplification

Analytical spectral design of mechanical metamaterials with inertia amplification

by Valeria Settimi[1]*, Marco Lepidi[2], Andrea Bacigalupo[2]

[1] *Department of Civil and Building Engineering and Architecture, Polytechnic University of Marche, Ancona, Italy*
[2] *Department of Civil, Chemical and Environmental Engineering, University of Genoa, Genoa, Italy*

*Corresponding author: v.settimi@staff.univpm.it

Analytical spectral design of mechanical metamaterials with inertia amplification

Valeria Settimi[a,*], Marco Lepidi[b], Andrea Bacigalupo[b]

[a] *DICEA - Dipartimento di Ingegneria Civile, Edile e Architettura, Università Politecnica delle Marche, Ancona (Italy)*
[b] *DICCA - Dipartimento di Ingegneria Civile, Chimica e Ambientale, Università di Genova, Genova (Italy)*

Abstract

Functional metamaterials offering superior dynamic performances can be conceived by introducing local mechanisms of inertia amplification in the periodic microstructure of cellular composite media. The minimal physical realization of an inertially amplified metamaterial is represented by a one-dimensional crystal lattice, characterized by an intracellular pantograph mechanism. The microstructural dynamics of the periodic tetra-atomic cell is synthetically described by a low-dimension lagrangian model. The lagrangian coordinates account for the longitudinal motion of a pair of elastically coupled principal atoms, rigidly connected by the pantograph arms to a pair of transversely-oscillating secondary atoms, serving as inertial amplifiers. Within the range of small-oscillations, the free propagation of undamped harmonic waves is described by a linear difference equation, governed by a symplectic transfer matrix. First, the band structure of the complex-valued dispersion spectrum is determined analytically, by properly exploiting the formal (time-to-space) analogy with the Floquet Theory for the stability of non-autonomous dynamic systems (*direct problem*). Second, a spectral design problem is stated and solved by inverting analytically the functions expressing parametrically the boundaries separating attenuation (stop) and propagation (pass) bands in the frequency spectrum (*inverse problem*). Specifically, the inverse problem solution has the merit of providing simple formulas for parametric design. Such formulas explicitly and exactly identify the mechanical parameters of the inertially amplified metamaterial possessing a desired pass-stop-pass band structure, assigned according to functional design requirements. The existence and uniqueness of the solution in the admissible range of mechanical parameters is discussed. The discussion provides (i) mathematical demonstration for the existence of feasible design solutions or multi-solutions, (ii) complete definition of the physically realizable band structures in the frequency domain, and (iii) alternative criteria to design iso-band structured metamaterials within the admissible domain of mechanical parameters. The extra-customization possibilities offered by iso-band structured metamaterials are analyzed in terms of static and dynamic performances. As feasible limit cases of the analytical spectral design, extreme mechanical metamaterials working as phononic superfilters and/or superpropagators are realizable.

Keywords: Periodic materials, Pantographic metamaterials, Wave propagation, Inverse problems, Parametric design, Material functionalization.

1. Introduction

Several theoretical and applied problems in solid and structural mechanics deal with the inverse problem of determining the physical parameters of a vibrating system, starting from complete or partial knowledge about its spectral properties [1–3]. Depending on the nature or origin of the known spectral information, at least two distinct classes of inverse problems have been traditionally distinguished and separately addressed in the scientific literature. The first class of problems essentially consists in identifying the inertial, geometric and elastic parameters of an existing dynamic system whose spectral data have been assessed experimentally, or pseudo-experimentally (*identification problem*). A complementary problem concerns the diagnosis of the mechanical degradation which can be deemed to cause measurable changes in the spectral data monitored over time (*model updating* and *damage identification problems*). The second class of problems essentially consists in determining the design variables of a realizable – if it exists – dy-

*Corresponding author
Email address: v.settimi@staff.univpm.it (Valeria Settimi)

namic system, whose spectral data have been assigned according to desired targets (*design problem*). Due to the inherent nonlinearity of the design problems, some key issues concerning the existence and uniqueness of the solution withing the physically compatible range of design variables must be discussed. If the solution does not exist, the problem statement can be upgraded to search for an alternative solution minimizing the difference with the incompatible design targets. Otherwise, if multiple solutions exist, the problem can be reformulated to maximize some extra design variables (*optimization* or *optimal design problems*).

The theoretical principles and research tools developed in the wide area of spectral design are currently being increasingly exploited in the rapidly emerging field of periodic architected materials. Specifically, different spectral design and optimization problems have been addressed for phononic crystals, beam lattices and mechanical metamaterials, either via analytical techniques [4–7], or by means of computational methods [8–16]. Besides methodological aspects, the motivating idea is that – compared with unstructured media – periodic architected materials offer a larger space of design variables, ranging from the cellular topology to the phase compositeness and, significantly, the microstructural parameters. With respect to the latter, a proper tuning of the geometrical and physical microproperties can allow the precise government of many dynamic phenomena characterized by wavelengths larger than the cellular size. Low-pass and high-pass wavefrequency filtering, directional energy transfers, waveform polarization and hybridization, negative refraction indexes, acoustic invisibility cloaking, amplitude-dependent dispersion relations, sub- and super-harmonic resonances are only a few examples of the fascinating functionalities that can be realized and governed by microstructurally designing the spectral properties of periodic media [17–25].

Within this challenging scenario, an emerging research trend is targeted at conceiving, modeling, analyzing and designing new mechanical metamaterials, realized by enriching the periodic microstructure of a cellular medium with local mechanisms operating at the cell scale, like local resonances, inertia amplification, multi-stability, and trampoline stiffness [26–29]. Among the others, inertial amplification can be realized by virtue of an intracellular (local) pantographic mechanism based on rhombic modules of rigid trusses connecting eccentric masses [30–32]. Interestingly, the local pantographic mechanism has been found to generate inertial nonlinearities in the equations governing the wave propagation [33]. From the mechanical viewpoint, the pantographic microstructural scheme grants a threefold advantage. Firstly, the rigidly-connected eccentric masses do not introduce additional active degrees-of-freedom and – consequently – do not enlarge the dimension of the periodic cell model. Secondly, the pantographic mechanism, being kinematically indeterminate, does not increase the microstructural stiffness and, therefore, does not alter the static performance of the metamaterial. Lastly, the mechanical linkage of hinged rigid bodies required to build up the pantographic scheme is easily realizable from a technological viewpoint [34]. The pantographic mechanisms of inertia amplification have been proved to be efficient in modifying the band structure of mechanical metamaterials, with particular efficiency in opening stop bands inhibiting the propagation of elastic waves [30, 35, 36]. This specific feature offers the opportunity to pursue both theoretical and applied objectives. The former task may consist in stating and solving inverse spectral problems, followed by a proper discussion about the data admissibility, and the solution existence and uniqueness. The latter task may consist in exploiting the problem solutions to design functional metadevices working as vibration filters or propagators for the frequency bands of interest. In this respect, obtaining *analytical* solution as explicit function of the microstructural parameters can be considered a remarkable and valuable achievement, aligned with the modern concepts of parametric design.

Based on this scientific background, the present paper considers a one-dimensional infinite lattice, characterized by a tetra-atomic periodic cell, realizing a minimal prototype of pantographic metamaterial with inertia amplification (Section 2). A linear discrete model is formulated to describe the free undamped dynamics of the cellular microstructure in the range of small amplitude oscillations (Subsections 2.1 and 2.2). The direct spectral problem of analytically determining the dispersion properties in the domain of real-valued frequencies and complex-valued wavenumbers is addressed by the transfer matrix method (Subsection 2.3). Therefore, the inverse spectral problem of analytically designing the microstructural parameters realizing a certain band structure is addressed (Section 3). First, a general strategy is defined to consistently state and parametrically solve the design problem, according to different possible criteria (Subsection 3.1). Second, the strategy is applied to exactly design the desired tri-band structure of the pantographic metamaterial (Subsection 3.2). Subsequently, the design procedure is extremized by imposing limit spectral conditions, corresponding to isoband structured spectra (Subsection 3.3), frequency superpropagation or superfiltration (Subsection 3.4). Finally, concluding remarks are pointed out.

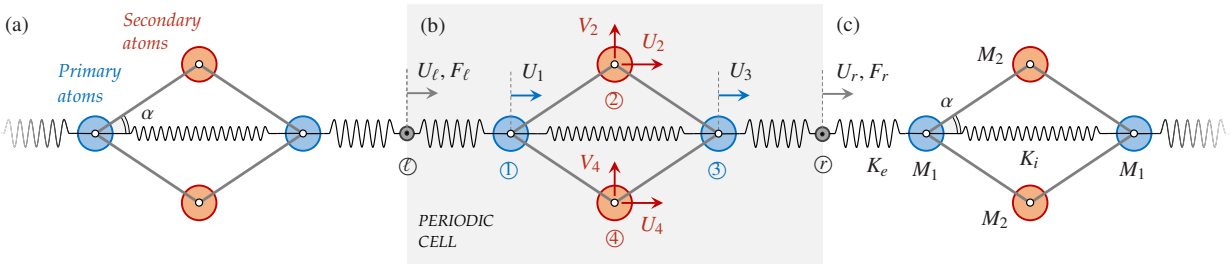

Figure 1: Periodic pantographic metamaterial [33]: (a) tetra-atomic unit, (b) periodic cell of the discrete model, (c) mechanical properties.

2. Pantographic metamaterial

A one-dimensional crystal lattice is considered as minimal paradigmatic model, representative of pantographic metamaterials $\mathcal{M}^p$ with inertia amplification (Figure 1a). The crystalline microstructure is physically realizable by synthesizing an infinite chain of identical massive disks (*primary atoms*), complemented by additional lateral massive disks (*secondary atoms*), symmetrically located on both sides of the chain axis. The secondary atoms are paired in correspondence of the mid-distance between alternate couples of primary atoms. Consequently, a repetitive tetra-atomic unit can be identified, characterized by two primary and two secondary atoms, spatially organized according to a rhombic scheme in the plane containing all the disk centroids (*metamaterial plane*). From the geometrical viewpoint, the rhombic shape of the repetitive unit is fully characterized by the distance L separating the primary atoms and the acute angle α between the chain axis and the primary-to-secondary atom alignments (*amplification angle*). Each primary atom is assumed to exchange only conservative position-dependent forces (attraction or repulsion) with the nearest-neighbor elements of the chain. Within a single unit, the key assumption of unchangeable mutual distance between each pair of primary-secondary atoms is introduced.

2.1. Mechanical discrete model

From the physical-mathematical viewpoint, the free undamped dynamics of the pantographic metamaterial can be adequately described by a parametric discrete formulation, which leads to a finite low-dimension mechanical model by virtue of the microstructural periodicity. According to this idea, all atoms are modeled as point masses located at the disk centroids, while the rhombic tetra-atomic unit is conveniently selected as periodic cell (Figure 1b). Consequently, the undeformed configuration of the reference microstructured cell is described by a set of four configurational nodes, located at the rhombus vertices. The respective masses M_1 and M_2 of the primary and secondary atoms are supposed to be different from each other, in the general case (Figure 1c). As fundamental hypothesis, the primary atoms are assumed to possess a single degree-of-freedom, corresponding to the translation along the chain axis. Differently, each secondary atom is supposed to develop a two degrees-of-freedom translation in the metamaterial plane. Within the reference cell, the unique degree-of-freedom of the two principal atoms is described by the displacements U_1 and U_3 of the configurational nodes ① and ③. Similarly, the two degrees-of-freedom of the secondary atoms are described by the displacement components U_2, U_4 and V_2, V_4 (respectively parallel and orthogonal to the chain axis) of the configurational nodes ② and ④. Auxiliary massless nodes ⓛ and ⓡ, characterized by a unique chain-aligned translational degree-of-freedom described by the displacements U_ℓ and U_r, are purposely introduced at the left and right sides of the cell boundary, respectively.

The inter-cellular and intra-cellular couplings among the principal atoms are simulated by inter-nodal linear elastic springs. Specifically, the inter-cellular interactions between the nearest principal atoms of two adjacent cells is simulated by a series of two equal-length springs with identical stiffness K_e (*external springs*). The intra-cellular interaction between the two principal atoms of the same cell is simulated by a single spring with stiffness K_i (*internal spring*). The constraint of unchangeable mutual distance between each pair of primary and secondary atoms is reproduced by a rigid truss link connecting the respective configurational nodes.

The ordinary differential equations governing the discrete model dynamics can be presented in a suited nondimensional form by defining the dimensionless

time $\tau = \Omega t$, where the quantity $\Omega^2 = K_e/M_1$ is selected as reference (square) frequency. Furthermore, adopting the distance L as reference length, the time-dependent dimensionless displacements can be defined

$$u_1 = \frac{U_1}{L}, \quad u_2 = \frac{U_2}{L}, \quad u_3 = \frac{U_3}{L}, \quad u_4 = \frac{U_4}{L} \qquad (1)$$
$$v_2 = \frac{V_2}{L}, \quad v_4 = \frac{V_4}{L}, \quad u_\ell = \frac{U_\ell}{L}, \quad u_r = \frac{U_r}{L}$$

and the positions $w = u_3 - u_1$ and $u = u_1$ are introduced for the sake of convenience. In particular, the variable w describes the dimensionless relative displacement between the primary atoms.

As major remark to establish the model dimension, the displacements u_ℓ and u_r can be recognized as *passive* degrees-of-freedom, associated to massless nodes that cannot develop inertial forces. Furthermore, all the displacements of the secondary atoms are requested to satisfy the internal constrain equation

$$u_2 = u_4 = u + \tfrac{1}{2}w, \qquad v_2 = -v_4 \qquad (2)$$

in order to respect the double-symmetry with respect to the geometrical center of the periodic cell. Finally, the indeformability conditions of the rigid truss links connecting the primary and secondary atoms impose the additional exact relation

$$v_4 = \tfrac{1}{2}\tan\alpha - \tfrac{1}{2}\left(1 + \tan^2\alpha - (1+w)^2\right)^{1/2} \qquad (3)$$

which states how, fixed a certain amplification angle α, the chain-orthogonal displacements v_4 and v_2 of the secondary atoms nonlinearly and exclusively depend on the chain-parallel relative displacement w of the primary atoms. It can be demonstrated that the relation (3) can be asymptotically expressed as $v_4 = \frac{1}{2}\cot\alpha\, w + O(w^2)$ in the small amplitude regime of w-oscillations.

A minimal set $\mathbf{p}$ of three independent dimensionless parameters, sufficient to completely describe the mechanical model, is composed by the quantities

$$\varrho^2 = \frac{M_2}{M_1}, \qquad \eta = \frac{K_i}{K_e} \qquad (4)$$

together with the amplification angle $\alpha \in (0, \pi/2)$. From the physical viewpoint, the parameter ϱ^2 describes the secondary-to-primary *mass ratio*, whereas the parameter η represents the internal-to-external *stiffness ratio*. Naturally, the mass and stiffness ratios must be assumed strictly positive ($\varrho^2 > 0$, $\eta > 0$).

2.2. Equations of motion

Adopting the undeformed configuration as initial reference for the dynamic equilibrium, the Hamilton's principle can be applied, considering also the symmetry and indeformability conditions (2) and (3). Therefore, within the approximation limits of the small amplitude regime of oscillations, the linearized ordinary differential equations governing the free undamped dynamics of the periodic cell read

$$2(1+\varrho^2)\ddot{u} + (1+\varrho^2)\ddot{w} + 2u + w - u_\ell - u_r = 0 \qquad (5)$$
$$(1+\varrho^2)\ddot{u} + (1+\varrho_e^2)\ddot{w} + u + (1+\eta)w - u_r = 0$$

where dot indicates differentiation with respect to dimensionless time. The relevant effect of inertia amplification can be recognized in the ϱ^2-dependent coefficients multiplying all the acceleration terms. In particular, the inertia term in the second equation can be further increased by regulating the amplification angle, since the α-dependent auxiliary parameter

$$\varrho_e^2 = \tfrac{1}{2}\varrho^2(1 + \cot^2\alpha) \qquad (6)$$

obeys to the rule $\varrho_e^2 > \varrho^2$ in the range $\alpha \in (0, \pi/4)$.

The Hamilton's principle returns also the linear equations governing the quasi-static equilibrium at the external nodes. Denoting by N_ℓ and N_r the restoring forces in the left and right secondary springs (tensions if $n_\ell > 0$ and $n_r > 0$), respectively, the equations read

$$n_\ell = u - u_\ell, \qquad n_r = u_r - u - w \qquad (7)$$

where the dimensionless quantities $n_\ell = N_\ell/(K_e L)$ and $n_r = N_r/(K_e L)$ are introduced. It may be worth noting that the same equations can be equivalently expressed in terms of the nondimensional external forces $f_\ell = -n_\ell$ and $f_r = n_r$ exerted at the left and right external nodes.

Collecting all the *active* displacements in the configurational coordinate vector $\mathbf{u}_a = (u, w)$ and all the *passive* displacements in the vector $\mathbf{u}_p = (u_\ell, u_r)$, the equations of motion (5) and the quasi-static equations (7) can conveniently be expressed in the matrix form

$$\mathbf{M}\ddot{\mathbf{u}}_a + \mathbf{K}_{aa}\mathbf{u}_a + \mathbf{K}_{ap}\mathbf{u}_p = \mathbf{0} \qquad (8)$$
$$\mathbf{K}_{pa}\mathbf{u}_a + \mathbf{K}_{pp}\mathbf{u}_p + \mathbf{n}_p = \mathbf{0}$$

where the mass and stiffness matrices are

$$\mathbf{M} = \begin{bmatrix} 2(1+\varrho^2) & 1+\varrho^2 \\ 1+\varrho^2 & 1+\varrho_e^2 \end{bmatrix}, \quad \mathbf{K}_{aa} = \begin{bmatrix} 2 & 1 \\ 1 & 1+\eta \end{bmatrix} \qquad (9)$$
$$\mathbf{K}_{ap} = \begin{bmatrix} -1 & -1 \\ 0 & -1 \end{bmatrix}, \quad \mathbf{K}_{pp} = \begin{bmatrix} 1 & 0 \\ 0 & -1 \end{bmatrix}$$

while the stiffness matrix $\mathbf{K}_{pa} = \mathbf{K}_{ap}^\top$ and the vector of passive restoring forces is $\mathbf{n}_p = (n_\ell, n_r)$.

2.3. Free wave propagation

In order to study harmonic motions, the linear equations (8) can be treated by employing the Fourier transform, which here applies to the generic m-dimensional time-dependent vector variable $\mathbf{x}(\tau):\mathbb{R}\to\mathbb{R}^m$ as the integral $\mathcal{F}[\mathbf{x}(\tau)]=\int_{-\infty}^{\infty}\mathbf{x}(\tau)\exp(-\imath\omega\tau)\mathrm{d}\tau=:\hat{\mathbf{x}}(\omega)$, where $\omega\in\mathbb{R}$ is a nondimensional circular frequency and the transformed variable $\hat{\mathbf{x}}(\omega):\mathbb{R}\to\mathbb{R}^m$. The Fourier transformed equations of motion read

$$\begin{aligned}\left(\mathbf{K}_{aa}-\omega^2\mathbf{M}\right)\hat{\mathbf{u}}_a+\mathbf{K}_{ap}\hat{\mathbf{u}}_p&=\mathbf{0}\\ \mathbf{K}_{pa}\hat{\mathbf{u}}_a+\mathbf{K}_{pp}\hat{\mathbf{u}}_p+\hat{\mathbf{n}}_p&=\mathbf{0}\end{aligned}\tag{10}$$

where transformed active and passive variables co-exist. Subsequently, a general solution strategy different from the traditional quasi-static condensation of the passive variables $\hat{\mathbf{u}}_p$ and $\hat{\mathbf{n}}_p$ can be implemented. Indeed, equation (10a) can be handled to express the active displacements as linear function of the passive displacements in the form $\hat{\mathbf{u}}_a=-(\mathbf{K}_{aa}-\omega^2\mathbf{M})^{-1}\mathbf{K}_{ap}\hat{\mathbf{u}}_p$. By virtue of this result, equation (10b) can be expressed as

$$\mathbf{K}(\omega)\hat{\mathbf{u}}_p+\hat{\mathbf{n}}_p=\mathbf{0}\tag{11}$$

where the passive variables play the role of principal unknowns and $\mathbf{K}(\omega)=[\mathbf{K}_{pp}-\mathbf{K}_{pa}(\mathbf{K}_{aa}-\omega^2\mathbf{M})^{-1}\mathbf{K}_{ap}]$ is the ω-dependent (condensed) stiffness matrix. Therefore, equation (11) can be expressed in the form

$$\begin{bmatrix}K_{\ell\ell} & K_{\ell r}\\ K_{r\ell} & K_{rr}\end{bmatrix}\begin{pmatrix}\hat{u}_\ell\\ \hat{u}_r\end{pmatrix}+\begin{pmatrix}\hat{n}_\ell\\ \hat{n}_r\end{pmatrix}=\begin{pmatrix}0\\ 0\end{pmatrix}\tag{12}$$

where explicit dependence of all the matrix components on the frequency ω is understood. Alternately, by suitably introducing two state vectors listing left and right passive variables $\hat{\mathbf{z}}_\ell=(\hat{u}_\ell,\hat{n}_\ell)$ and $\hat{\mathbf{z}}_r=(\hat{u}_r,\hat{n}_r)$, equation (11) takes the form of a difference equation

$$\hat{\mathbf{z}}_r=\mathbf{T}(\omega)\hat{\mathbf{z}}_\ell\tag{13}$$

where the two-by-two *transfer matrix* $\mathbf{T}(\omega)$, relating the left and right passive variables, reads

$$\mathbf{T}(\omega)=\begin{bmatrix}-K_{\ell r}^{-1}K_{\ell\ell} & -K_{\ell r}^{-1}\\ K_{rr}K_{\ell r}^{-1}K_{\ell\ell}-K_{r\ell} & K_{rr}K_{\ell r}^{-1}\end{bmatrix}\tag{14}$$

and can be proved to be symplectic. Equation (13) states that two natural motions exist in the form of freely propagating waves $\hat{\mathbf{z}}_r=\exp(\imath\beta)\hat{\mathbf{z}}_\ell$, where β plays the role of ω-dependent wavenumber or propagation constant. Indeed, the free wave motions solve the eigenproblem

$$(\mathbf{T}(\omega)-\mu\mathbf{I})\hat{\mathbf{z}}_\ell=\mathbf{0}\tag{15}$$

where the eigenvalue $\mu=\exp(\imath\beta)$. By virtue of the symplecticity, the transfer matrix has unitary determinant and reciprocal eigenvalues. Consequently, the characteristic polynomial is palindromic

$$P(\mu)=\mu^2+\mathcal{J}(\omega)\mu+1\tag{16}$$

and the only non-unitary invariant coefficient $\mathcal{J}(\omega)$ suffices to fully characterize the propagation properties of the periodic system. The characteristic equation $P(\mu)=0$ can be solved to determine the eigenvalues

$$\mu_{1,2}(\omega)=-\tfrac{1}{2}\mathcal{J}(\omega)\pm\tfrac{1}{2}\left(\mathcal{J}(\omega)^2-4\right)^{1/2}\tag{17}$$

which can be proved to be reciprocal, that is $\mu_2=\mu_1^{-1}$.

Once the two eigenvalues μ_1 and μ_2 are known, the relation $\mu=\exp(\imath\beta)$ can be inverted to determine the *dispersion relations* in the (inverse) form

$$\beta(\omega)=\arg\left(\mu(\omega)\right)-\tfrac{1}{2}\imath\log\left(|\mu(\omega)|^2\right)\tag{18}$$

relating the real-valued frequency ω to the wavenumber β, which can be either real-valued (*propagating* waves) or imaginary-valued (*non-propagating* waves). Finally, inverting the relation (18) allows expressing the dispersion functions is the traditional (direct) form $\omega(\beta)$.

The essential role played by the invariant coefficient $\mathcal{J}(\omega)$ in determining the band structure of the periodic system can be unveiled by invoking the formal analogy with the Floquet theory for the stability of dynamical systems [37–39]. Indeed, depending on the coefficient $\mathcal{J}(\omega)$, three fundamental cases can occur

i) μ_1,μ_2 complex conjugates if $-2<\mathcal{J}(\omega)<2$,

ii) μ_1,μ_2 real and distinct if $\mathcal{J}(\omega)<-2\cup\mathcal{J}(\omega)>2$,

iii) μ_1,μ_2 real and coincident if $\mathcal{J}(\omega)=\pm2$.

With reference to the characteristic equation, these three cases correspond to: (i) complex-valued roots μ_1,μ_2 sitting on the unitary circle of the complex plane, identifying *pass bands* in the frequency axis (the analogous of stable regions corresponding to elliptic fixed points), (ii) real-valued roots μ_1,μ_2 lying inside and outside the unitary circle of the complex plane, respectively, and identifying *stop bands* in the frequency axis (the analogous of unstable regions corresponding to hyperbolic or reflective hyperbolic fixed points), (iii) real valued and coincident roots μ_1,μ_2 sitting on the unitary circle of the complex plane, identifying boundaries between pass and stop bands (the analogous of bifurcation loci corresponding to parabolic fixed points) and also defining the upper and lower edges of each band. It may be worth noting that, in the absence of damping, the roots μ_1,μ_2 of the fundamental case (i) are purely imaginary.

For the particular pantographic metamaterial under investigation, the invariant coefficient reads

$$\mathcal{J}(\omega) = \frac{2\left(2\eta - \varrho^2\omega^2 \csc^2\alpha\right)\left(r_1\omega^2 - 1\right) + 4\omega^2\left(r_2\omega^2 + 1\right)}{2\eta + \varrho^2\omega^2(1 - \cot^2\alpha)} \tag{19}$$

where $r_1 = 2(\varrho^2+1)$ and $r_2 = \varrho^4 - 1$. Therefore, imposing $\mathcal{J}(\omega) = \pm 2$ to satisfy the condition (iii) allows determining the $(\omega, \mathbf{p})$-loci in the frequency-parameter space corresponding to the transition between the pass and stop regions. Specifically, the locus satisfying the subcondition $\mathcal{J}(\omega) = 2$ can be defined by two bounding functions $\omega_1^2(\mathbf{p}), \omega_2^2(\mathbf{p})$, while the locus satisfying the subcondition $\mathcal{J}(\omega) = -2$ can be defined by two bounding functions $\omega_3^2(\mathbf{p}), \omega_4^2(\mathbf{p})$. It can be verified that $\omega_4^2(\mathbf{p}) = 0$, whereas the other bounding functions are

$$\begin{aligned} \omega_1^2(\mathbf{p}) &= \frac{1}{1+\varrho^2}, \\ \omega_2^2(\mathbf{p}) &= \frac{4\eta \sin^2\alpha}{1+\varrho^2+(1-2\sin^2\alpha)(\varrho^2-1)}, \\ \omega_3^2(\mathbf{p}) &= \frac{(1+2\eta)\sin^2\alpha}{\varrho^2+(1-\varrho^2)\sin^2\alpha}. \end{aligned} \tag{20}$$

Moreover, the locus $\mathcal{T}_{ss}$ corresponding to the vanishing of the $\mathcal{J}(\omega)$-denominator is associated to the boundary separating two stop subregions (from hyperbolic to reflective hyperbolic fixed points or viceversa in the analogy with the Floquet theory).

The pass and stop regions separated by the surfaces described by the bounding functions $\omega_1(\mathbf{p})$ (red), $\omega_2(\mathbf{p})$ (orange) and $\omega_3(\mathbf{p})$ (green) over the parameter space (η, ϱ^2) are illustrated in Figure 2a for the amplification angle $\alpha = \pi/8$. The pass region (yellow-filled) is composed by a low-frequency acoustic band and a high-frequency optical band, separated by a single stop region (not filled), or frequency band gap. Fixing the stiffness ratio $\eta = 1$ (planar section S), the band structure versus the mass ratio ϱ^2 is portrayed in Figure 2b. The pass bands (yellow regions) and the stop bands (gray subregions), separated by the three bounding functions, can be distinguished. The curve corresponding to the locus $\mathcal{T}_{ss}$ within the stop band is identified (dashed red line). Two significant crossing points satisfying the conditions $\omega_1 = \omega_3$, corresponding to null optical bandwidth (at mass ratio ϱ_p^2), and $\omega_1 = \omega_2$, corresponding to null stop bandwidth (at mass ratio ϱ_s^2) are also marked (black dots). For each region, the position of the Floquet multipliers μ_1, μ_2 with respect to the unitary circle in the complex plane is qualitatively sketched. A selection of complex-valued spectra illustrating the dispersion functions $\omega(\beta)$ for selected ϱ^2-values is also reported (Figures 2c-g). The spectra are characterized by propagation curves in the $(\omega, \Re(\beta))$-plane (blue lines), covering the frequency range of the pass bands, and attenuation curves in the $(\omega, \Im(\beta))$-plane (red lines), covering the frequency range of the stop bands. An in-depth parametric analysis of the linear dispersion properties, considering also the spectral effects of varying the amplification angle α, is reported and discussed in [33].

3. Analytical spectral design

From the mathematical viewpoint, the analytical spectral design can be classified as an inverse eigenproblem, consisting in determining the particular set $\mathbf{p}$ of mechanical parameters (*unknowns*, or *design variables*) defining a specific material $\mathcal{M}$ characterized by a certain assigned band structure $\boldsymbol{\varpi}$ (*data*, or *design targets*). Solutions to the inverse eigenproblem are sought for in analytical (non numerical) and parametric (non topological) form $\mathbf{p}(\boldsymbol{\varpi})$. As valuable consequence, analytical solutions – if they can be found (exactly or possibly in a suited asymptotically approximate form) – can straightforwardly undergo parametric post-processes, including sensitivity analyses and functional optimizations.

Data. The target band structure can univocally be assigned by fixing the vector $\boldsymbol{\varpi} = (\varpi_1, ..., \varpi_j, ..., \varpi_n)$, listing the *spectral bounds* ϖ_j, corresponding to the maximal frequencies of n consecutive pass and stop bands, sorted in ascending order (with $\varpi_j \in \mathbb{R}_*^+$ and n not larger than the cellular model dimension). Equivalently, the target band structure can univocally be assigned by fixing the *spectral amplitudes* Δ_j (*amplitude-based design*), corresponding to the n pass and stop bandwidths. Clearly, the spectral bounds ϖ_j are associated to the spectral amplitudes Δ_j and the respective centerfrequencies σ_j by the relations $\Delta_j = \varpi_j - \varpi_{j-1}$ and $\sigma_j = \frac{1}{2}(\varpi_j + \varpi_{j-1})$, for $j = 1, .., n$ and setting $\varpi_0 = 0$.

Unknowns. In principle, the design variables can include the full set $\mathbf{p}$ of independent mechanical parameters defining the material microstructures. However, technical and/or technological requirements may reduce the number of free design variables or – most of the time – limit the admissible range of the solution, according to single-parameter or multi-parameter inequalities $\mathbf{h}(\mathbf{p}) \leq \mathbf{0}$. Within the admissible range, the solution may be not unique, or may even not exist, because the inverse eigenproblem is inherently nonlinear but also – after linearization – overdetermined or undetermined, in the general case. Therefore, the uniqueness of the solution – if it exists – is a key issue to be discussed.

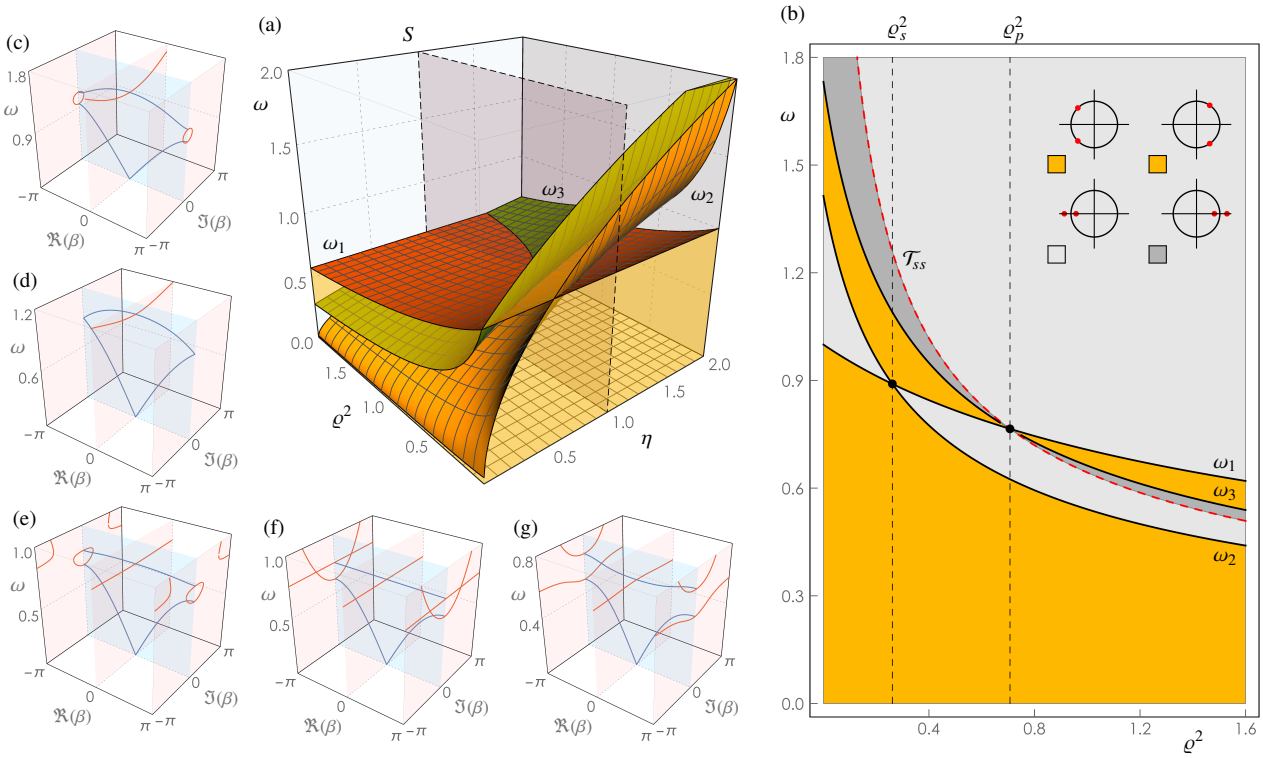

Figure 2: Dispersion properties of the pantographic metamaterial: (a) pass and stop regions separated by the bounding functions $\omega_1(\mathbf{p})$ (red), $\omega_2(\mathbf{p})$ (orange) and $\omega_3(\mathbf{p})$ (green) over the parameter space (η, ϱ^2) for the amplification angle $\alpha = \pi/8$, (b) band structure versus the mass ratio ϱ^2 for stiffness ratio $\eta = 1$. Complex-valued spectra with dispersion curves (blue branches lying in the light blue plane) and attenuation curves (red branches lying in the light red planes) for the mass ratios: (c) $\varrho^2 = 9/100$, (d) $\varrho^2 = \varrho_s^2$, (e) $\varrho^2 = 60/100$, (f) $\varrho^2 = \varrho_p^2$, (g) $\varrho^2 = 121/100$.

In this respect, non-uniqueness (*iso-spectral* solutions) can be regarded as a valuable resource, offering equally-performing alternatives to the designer.

The strategy of spectral design outlined in the following is formulated for generic mono-coupled periodic systems described by a two-dimensional cellular model, featuring a tri-band dispersion spectrum. Consequently, the target band structure can be assigned by fixing the vector $\boldsymbol{\varpi} = (\varpi_1, \varpi_2, \varpi_3)$, where the three spectral bounds $\varpi_1, \varpi_2, \varpi_3$ correspond to the maximal frequencies of the acoustic pass band, stop band and optical pass band, respectively. The vector $\boldsymbol{\varpi}$ must be selected in the data domain $\mathfrak{V} := \{\boldsymbol{\varpi} : \varpi_3 > \varpi_2 > \varpi_1 > 0\}$. In order to stress the physical meaning of the spectral bounds, it may be convenient to introduce the positions $\varpi_a := \varpi_1$ (referred to as the *acoustic bound*), $\varpi_g := \varpi_2$ (*gap bound*), $\varpi_o := \varpi_3$ (*optical bound*). The respective spectral amplitudes in the vector $\boldsymbol{\Delta} = (\Delta_1, \Delta_2, \Delta_3)$ can conveniently be referred to as $\Delta_a := \Delta_1$ (*acoustic bandwidth*), $\Delta_g := \Delta_2$ (*stop bandwidth*), and $\Delta_o := \Delta_3$ (*optical bandwidth*), defined according to the relation

$$\Delta_a = \varpi_a, \qquad \Delta_g = \varpi_g - \varpi_a, \qquad \Delta_o = \varpi_o - \varpi_g \tag{21}$$

where the vector $\boldsymbol{\Delta}$ must be selected in the data domain $\mathfrak{V} := \{\boldsymbol{\Delta} : \Delta_a > 0 \wedge \Delta_g > 0 \wedge \Delta_o > 0\}$. Exact parametric solutions of the inverse eigenproblem are achievable in the specific application to the pantographic metamaterial.

3.1. Parametric inverse problem

Ideally, the analytical solution of the direct eigenproblem governing the dispersion properties of a periodic one-dimensional material gives the dispersion relations $\omega(\mathbf{p}, \beta)$ as explicit functions of all the mechanical parameters $\mathbf{p}$ *and* the wavenumber β. More feasibly, solving the direct eigenproblem associated to the transfer matrix $\mathbf{T}(\omega)$ allows determining analytically the β-independent *bounding functions* $\omega_i(\mathbf{p})$ expressing the $\mathbf{p}$-dependent boundaries separating the frequency bands.

Knowing the high-level information represented by the β-dependent relations $\omega(\mathbf{p}, \beta)$ is necessary only if the spectral analytical design requires the identification of a material possessing a desired spectral component at a certain wavenumber [5]. To the purpose of the inverse problem under investigation, finalized at the analytical design of the spectral band structure, the low-level information represented by the β-independent bounding

functions $\omega_i(\mathbf{p})$ is sufficient. Indeed, if the double condition $\mathcal{J}(\omega) = \pm 2$ admits four analytical solutions in the (square) frequency $\omega_i^2(\mathbf{p})$, for $i = 1, .., 3$ (since the forth solution is identically null), the essential outcome of the direct problem is the parametric vector function

$$\boldsymbol{\omega}^2(\mathbf{p}) = (\omega_1^2(\mathbf{p}), \omega_2^2(\mathbf{p}), \omega_3^2(\mathbf{p})) \tag{22}$$

listing the *spectral bounding functions* $\omega_1^2(\mathbf{p})$, $\omega_2^2(\mathbf{p})$, $\omega_3^2(\mathbf{p})$. The fundamental issue, which makes the spectral design problem not trivial, is that the spectral bounds evaluated according to the functions $\omega_i^2(\mathbf{p})$ cannot be presumed to be automatically sorted in ascending order over the entire space of the mechanical parameters $\mathbf{p}$. To exemplify, the first and last functions $\omega_1^2(\mathbf{p})$ and $\omega_3^2(\mathbf{p})$ can mathematically be verified not to systematically describe the lowest and highest spectral bounds for all the admissible parameter sets $\mathbf{p} \in \mathfrak{U}$ (see also Figure 2). This natural condition is conventionally referred to as *unsorting* (absence of a systematic sorting order) in the following. Due to the unsorting, the three spectral bounding functions $\omega_i^2(\mathbf{p})$ cannot be univocally associated to the ordered (square) acoustic bound ϖ_a^2, gap bound ϖ_g^2, optical bound ϖ_o^2. Although the unsorting is undoubtedly a factor complicating the inversion of the direct eigenproblem (*problem inversion*), it nevertheless offers a multiplicity of solution schemes for the inverse problem (*design criteria*).

Problem inversion. According to the above considerations, the inverse problem can be formalized by assigning known values (design targets) to the bounding functions $\boldsymbol{\omega}^2(\mathbf{p}) : \mathfrak{A} \to \mathbb{R}_+^3$, where $\mathfrak{A} = \{\mathbf{p} \in \mathbb{R}^n : \mathbf{h}(\mathbf{p}) \leq \mathbf{0}\}$ stands for the admissibility domain of the n-dimension parameter set $\mathbf{p}$. To this purpose, the conundrum of assigning known (i.e. *a priori sorted*, or *sortable*) data to unsorted (i.e. *non univocally sortable* in $\mathfrak{A}$) bounding functions can properly be bypassed by introducing an auxiliary set $\mathbf{d} = (d_1, d_2, d_3) \in \mathbb{R}_+^3$, listing three auxiliary target quantities d_1, d_2, d_3 in a generic (i.e. *not necessarily sorted*) order. Therefore, the governing *design equation* can be imposed in the form $\boldsymbol{\omega}^2(\mathbf{p}) = \mathbf{d}$. Finally, the design equation can – ideally – be analytically inverted to obtain the explicit relation $\mathbf{p} = \mathbf{g}(\mathbf{d}) : \mathbb{R}_+^3 \to \mathfrak{A}$, providing the sought solution of the inverse problem as analytical function of the data. The *uniqueness* of the solution is generally guaranteed if the design equation is linear, or linearizable, and the number of unknowns $\mathbf{p}$ equals the number of data $\mathbf{d}$ (namely if $n = 3$). The *existence* of the solution within the admissible domain $\mathfrak{A}$ of the parameters is a complementary but fundamental problem, governed by the *compatibility condition*

$$\mathbf{f}(\mathbf{d}) := \mathbf{h}(\mathbf{g}(\mathbf{d})) \leq \mathbf{0} \tag{23}$$

stating that the solution-admitting (compatible) data $\mathbf{d}$ cannot be assigned arbitrarily, but are required to satisfy parameter-independent inequalities. It must be noted that the problem invertibility, as well as the solution uniqueness and existence, are case-specific matters, that is, they depend on the particular periodic material under investigation. As major remark, the inequality (23) defines the *compatibility domain* $\mathfrak{D} = \{\mathbf{d} \in \mathbb{R}^3 : \mathbf{f}(\mathbf{d}) \leq \mathbf{0}\}$, establishing the range of spectral design targets that are physically realizable for a certain periodic material $\mathcal{M}$.

Design criteria. Employing the auxiliary $\mathbf{d}$-quantities is functional at transforming the non-univocal association ϖ_i-to-ω_i into the equivalent association ϖ_i-to-d_i, which is still non-univocal, but allows an univocal statement of the design equation $\boldsymbol{\omega}^2(\mathbf{p}) = \mathbf{d}$. Although not mandatory, the advantage of this transformation is the valuable opportunity of post-treating the multiplicity of possible associations ϖ_i-to-ω_i *after* the solution of the inverse problem. Particularly, multiple inversions of the different direct problems that rise up from each possible association ϖ_i-to-ω_i are unnecessary. From a general perspective, this strategy may become fundamental if the number of different possible associations ϖ_i-to-ω_i (growing proportionally to the factorial $n!$) is large. In this respect, the enumeration and identification of all the possible associations ϖ_i-to-ω_i can conveniently be performed by defining a *sorting* generalized function $\mathbf{c}(\boldsymbol{\omega}^2)$. For the specific three band dispersion spectrum the sorting function reads by components

$$\begin{aligned} c_1(\boldsymbol{\omega}^2) &= \min\left[\omega_1^2, \omega_3^2\right] \\ c_2(\boldsymbol{\omega}^2) &= \min\left[\omega_1^2, \omega_2^2\right] \\ c_3(\boldsymbol{\omega}^2) &= \min\left[\omega_2^2, \omega_3^2\right] \end{aligned} \tag{24}$$

and properly distinguishes all the possible orders in which the three bounding functions $\omega_1^2, \omega_2^2, \omega_3^2$ can mathematically *and* physically be sorted in the parameter space. On the one hand, from the purely mathematical viewpoint, the function $\mathbf{c}(\boldsymbol{\omega}^2)$ admits six different and not self-contradicting outputs

$$\begin{aligned} \mathbf{c}_A &= (\omega_1^2, \omega_1^2, \omega_2^2) \quad \to \quad \mathfrak{a}_A(\boldsymbol{\omega}^2) = (\omega_1^2, \omega_2^2, \omega_3^2) \\ \mathbf{c}_B &= (\omega_1^2, \omega_2^2, \omega_2^2) \quad \to \quad \mathfrak{a}_B(\boldsymbol{\omega}^2) = (\omega_2^2, \omega_1^2, \omega_3^2) \\ \mathbf{c}_C &= (\omega_3^2, \omega_2^2, \omega_2^2) \quad \to \quad \mathfrak{a}_C(\boldsymbol{\omega}^2) = (\omega_2^2, \omega_3^2, \omega_1^2) \\ \mathbf{c}_D &= (\omega_1^2, \omega_1^2, \omega_3^2) \quad \to \quad \mathfrak{a}_D(\boldsymbol{\omega}^2) = (\omega_1^2, \omega_3^2, \omega_2^2) \\ \mathbf{c}_E &= (\omega_3^2, \omega_1^2, \omega_3^2) \quad \to \quad \mathfrak{a}_E(\boldsymbol{\omega}^2) = (\omega_3^2, \omega_1^2, \omega_2^2) \\ \mathbf{c}_F &= (\omega_3^2, \omega_2^2, \omega_3^2) \quad \to \quad \mathfrak{a}_F(\boldsymbol{\omega}^2) = (\omega_3^2, \omega_2^2, \omega_1^2) \end{aligned} \tag{25}$$

where the bijection $\mathfrak{a}_J(\boldsymbol{\omega}^2)$ from the set $\boldsymbol{\omega}^2$ in itself sorts the bounding functions ω_i in the ascending order uni-

vocally defined by the output $\mathbf{c}_J$, with $J = A, ..., F$. According to the rules of elementary combinatorics, the outputs of the functions $\mathfrak{a}_J(\boldsymbol{\omega}^2)$ coincide with all the six permutations (without repetitions) of the $\boldsymbol{\omega}^2$-set. On the other hand, from a physical viewpoint, it is likely that some permutations should be disregarded, because of their natural inconsistency. Specifically, physical inconsistency occurs when one or more generalized functions $c_i(\boldsymbol{\omega}^2)$ have a *single* possible output, by virtue of the known (but case-specific) dependence of the bounding functions $\omega_i^2(\mathbf{p})$ on the parameters of the particular material under investigation. Each permutation $\mathfrak{a}_J(\boldsymbol{\omega}^2)$ in the list (25) that is physically consistent for a certain periodic material $\mathcal{M}$ (i.e. corresponding to a non disregarded output of the functions (24)) gives an admissible univocal association ϖ_i-to-ω_i. Mathematically, each univocal association ϖ_i-to-ω_i can be expressed in the direct form $\boldsymbol{\varpi}^2 = \mathfrak{a}_J(\boldsymbol{\omega}^2)$ or – being the functions $\mathfrak{a}_J(\boldsymbol{\omega}^2)$ invertible – in the inverse form $\boldsymbol{\omega}^2 = \mathfrak{b}_J(\boldsymbol{\varpi}^2)$, where the vector $\boldsymbol{\varpi}^2 = \{\varpi_1^2, \varpi_2^2, \varpi_3^2\}$ has been introduced. Equivalently, but more conveniently, the admissible associations ϖ_i-to-d_i can be expressed as $\mathbf{d} = \mathfrak{b}_J(\boldsymbol{\varpi}^2)$, having set the design equations in the form $\boldsymbol{\omega}^2(\mathbf{p}) = \mathbf{d}$. Different admissible associations eventually correspond to alternative feasible *design criteria*, individually referred to as *Criterion J* in the following (with $J = A, B, C, ...$).

Fixed the association $\mathbf{d} = \mathfrak{b}_J(\boldsymbol{\varpi}^2)$ related to the consistent criterion J, the corresponding compatibility domain is defined as $\mathfrak{D}_J = \{\boldsymbol{\varpi}^2 \in \mathfrak{W}^2 : \mathbf{f}_J(\boldsymbol{\varpi}^2) := \mathbf{f}(\mathfrak{b}_J(\boldsymbol{\varpi}^2)) \leq \mathbf{0}\}$, where the space $\mathfrak{W}^2 := \{\boldsymbol{\varpi}^2 : \varpi_3^2 > \varpi_2^2 > \varpi_1^2 > 0\}$. From the theoretical viewpoint, the compatibility domains $\mathfrak{D}_J$ contains all (and only) the $\boldsymbol{\varpi}^2$-points describing band structures $\boldsymbol{\varpi}$ physically realizable according to the Criterion J. Conversely, from the operational viewpoint, a particular band structure $\boldsymbol{\varpi}$ can be physically realized according to the Criterion J only if the corresponding $\boldsymbol{\varpi}^2$-point is member of $\mathfrak{D}_J$. The compatibility domains $\mathfrak{D}_J$ are in general different from each other and can have non-null intersection. Consequently, a point $\boldsymbol{\varpi}^2$ that is member of two or more intersecting domains $\mathfrak{D}_J$ gives the designer the valuable opportunity to realize the same band structure $\boldsymbol{\varpi}$ according to different criteria. Precisely, the non null intersection $\mathfrak{D}_k$ of k different domains – if it exists – collects the points $\boldsymbol{\varpi}$ describing band structures physically realizable according to k different criteria. It is worth noting that analytically determining the domains $\mathfrak{D}_J$ allows describing the entire family of physically realizable band structures, including the most extreme design targets.

3.2. Design of the pantographic metamaterial

For the pantographic metamaterial $\mathcal{M}^p$ the spectral bounding functions are the three analytical parametric relations (20). Among the others, a convenient choice of the design variables is represented by the three independent nondimensional mechanical parameters collected in the vector $\mathbf{p} = (\eta, \varrho^2, \sin^2\alpha) \in \mathbb{R}^3_+$. Therefore, with respect to the problem inversion, the number of unknowns equates the number of design equations $\boldsymbol{\omega}^2(\mathbf{p}) = \mathbf{d}$. Moreover, notwithstanding the nonlinear nature of the design equations, an analytical solution $\mathbf{p} = \mathbf{g}(\mathbf{d})$ can be achieved, reading

$$\begin{aligned} \eta &= g_1(\mathbf{d}) = \frac{d_2}{2(d_3 - d_2)} \\ \varrho^2 &= g_2(\mathbf{d}) = \frac{1 - d_1}{d_1} \\ \sin^2\alpha &= g_3(\mathbf{d}) = \frac{(d_1 - 1)(d_3 - d_2)}{(2d_1 - 1)(d_3 - d_2) - d_1} \end{aligned} \tag{26}$$

which are denoted as *design formulas* in the following. The solution can be proved to be unique.

With respect to the design criteria, from the spectral bounding functions (20) of the pantographic metamaterial $\mathcal{M}^p$ it is possible to mathematically demonstrate that $\forall \mathbf{p}$ inequality $\omega_3^2(\mathbf{p}) > \omega_2^2(\mathbf{p})$ holds. Therefore, the generalized function $c_3(\boldsymbol{\omega}^2)$ defined in (24) has the single possible output ω_2^2. Consequently, the only physically consistent outputs in (25) are

$$\begin{aligned} \mathbf{c}_A &= (\omega_1^2, \omega_1^2, \omega_2^2) \\ \mathbf{c}_B &= (\omega_1^2, \omega_2^2, \omega_2^2) \\ \mathbf{c}_C &= (\omega_3^2, \omega_2^2, \omega_2^2) \end{aligned} \tag{27}$$

which allow the definition of three feasible design criteria. Specifically, once the band structure $\boldsymbol{\varpi} \in \mathbb{R}^3_+$ is assigned as design target

- *Criterion A*: consists in imposing the association $\boldsymbol{\varpi}^2 = \mathfrak{a}_A(\boldsymbol{\omega}^2)$, corresponding to conveniently setting in the inverse problem solution (26) the ϖ_i-to-d_i association $\mathbf{d} = \mathfrak{b}_A(\boldsymbol{\varpi}^2)$, reading in components

$$d_1 = \varpi_a^2, \qquad d_2 = \varpi_g^2, \qquad d_3 = \varpi_o^2 \tag{28}$$

- *Criterion B*: consists in imposing the association $\boldsymbol{\varpi}^2 = \mathfrak{a}_B(\boldsymbol{\omega}^2)$, corresponding to conveniently setting in the inverse problem solution (26) the ϖ_i-to-d_i association $\mathbf{d} = \mathfrak{b}_B(\boldsymbol{\varpi}^2)$, reading in components

$$d_1 = \varpi_g^2, \qquad d_2 = \varpi_a^2, \qquad d_3 = \varpi_o^2 \tag{29}$$

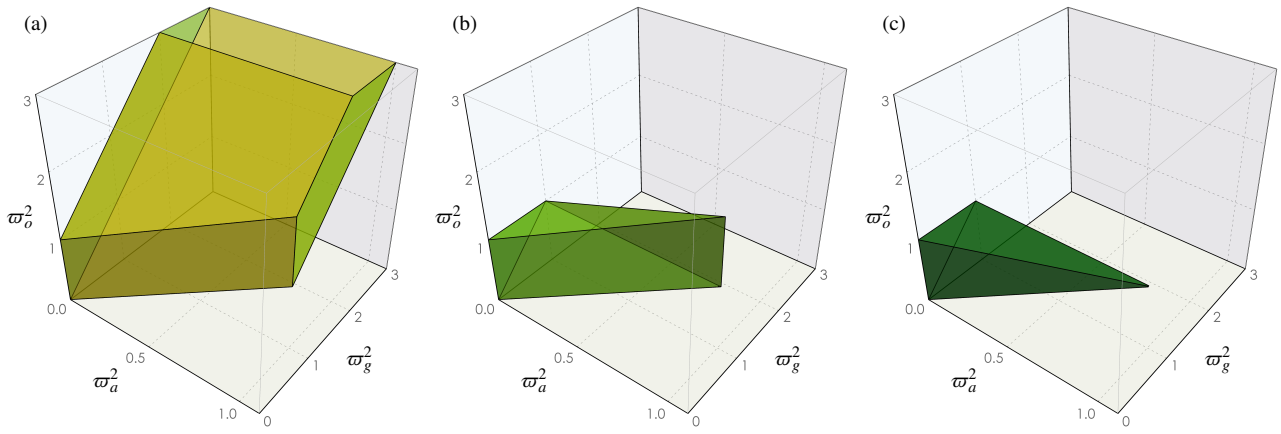

Figure 3: Three-dimensional domains of spectral compatibility in the space of (square) spectral bounds $\boldsymbol{\varpi}^2 = \{\varpi_a^2, \varpi_g^2, \varpi_o^2\}$: (a) domain $\mathfrak{D}_A$ compatible with *Criterion A*, (b) domain $\mathfrak{D}_B$ compatible with *Criterion B*, (c) domain $\mathfrak{D}_C$ compatible with *Criterion C*.

- *Criterion C*: consists in imposing the association $\boldsymbol{\varpi}^2 = \mathfrak{a}_C(\boldsymbol{\omega}^2)$, corresponding to conveniently setting in the inverse problem solution (26) the ϖ_i-to-d_i association $\mathbf{d} = \mathfrak{b}_C(\boldsymbol{\varpi}^2)$, reading in components

$$d_1 = \varpi_o^2, \qquad d_2 = \varpi_a^2, \qquad d_3 = \varpi_g^2 \tag{30}$$

Imposing the association $\mathbf{d} = \mathfrak{b}_J(\boldsymbol{\varpi}^2)$ according to one or the other set of equations (28)-(30), the solution of the design equation can be specialized for the criterion J by defining $\mathbf{g}_J(\boldsymbol{\varpi}^2) := \mathbf{g}(\mathfrak{b}_J(\boldsymbol{\varpi}^2))$. Consequently, the design formulas (26) read in components

$$\eta = g_{J1}(\boldsymbol{\varpi}^2), \quad \varrho^2 = g_{J2}(\boldsymbol{\varpi}^2), \quad \sin^2\alpha = g_{J3}(\boldsymbol{\varpi}^2) \tag{31}$$

according to the criterion J (with $J = A, B, C$). Therefore, although the analytical solution (26) of the design equation is unique (when expressing the unknown $\mathbf{p}$ as a function of the data $\mathbf{d}$), the inverse spectral problem admits three different design formulas (that express the unknown $\mathbf{p}$ as a function of the *sorted* data, that is, the spectral bounds $\boldsymbol{\varpi}$), one for each different criterion.

The inverse problem solution achieved analytically must eventually be discussed with regard to the compatibility issue. Specifically, the solution is required to satisfy proper physical conditions involving the mechanical parameters characterizing the metamaterial $\mathcal{M}^p$. A system of compatibility conditions $\mathbf{h}(\mathbf{p}) \leq \mathbf{0}$ suited for the mechanical model is expressed by the inequalities

$$\begin{aligned} &0 < \eta < \eta_{\max} \\ &0 < \varrho^2 < \varrho^2_{\max} \\ &0 < \sin^2\alpha < \sin^2\alpha_{\max} \end{aligned} \tag{32}$$

with $\alpha_{\max} = \pi/2$, while $\eta_{\max}$ and $\varrho^2_{\max}$ can generally be set as large as the technical possibilities allow, depending – case by case – on the available microstructural materials, high-precision engineering technologies and high-fidelity manufacturing instruments. Once imposed on the design formulas (31), inequalities (32) determine the compatibility domains $\mathfrak{D}_J \subset \mathbb{R}^3_+$ restricting the assignable range of the data, that is, the realizable band structures $\boldsymbol{\varpi}$ according to the criterion J. Alternately, if the amplitude-based design is adopted, the $\boldsymbol{\varpi}$-to-$\boldsymbol{\Delta}$ relations (21) can be employed to assess the compatibility domains $\mathfrak{B}_J \subset \mathbb{R}^3_+$ restricting the realizable $\boldsymbol{\Delta}$-amplitude band structures according to the Criterion J.

The compatibility domains $\mathfrak{D}_J$ can be portrayed and discussed within the space of (square) spectral bounds $\boldsymbol{\varpi}^2$, as illustrated in Figure 3. From the geometric viewpoint, all domains $\mathfrak{D}_J$ are three-dimensional simply-connected convex regions, either bounded ($\mathfrak{D}_B$ and $\mathfrak{D}_C$) or unbounded ($\mathfrak{D}_A$). The boundaries $\partial\mathfrak{D}_J$ are composed by planar surfaces delimited by straight edges. Since all the planar surfaces are mathematically defined by strict inequalities in equation (32) or in the $\mathfrak{W}^2$-definition, the boundary $\partial\mathfrak{D}_J$ does not belong to the domain $\mathfrak{D}_J$. From the physical viewpoint, only the acoustic bound has a common superior limit ($\varpi_a^2 < 1$) for all the Criteria. Differently, the gap and the optical bounds have a superior limit only for the domains $\mathfrak{D}_B$ (where $\varpi_g^2 < 1$ and $\varpi_o^2 < 2$) and $\mathfrak{D}_C$ (where $\varpi_g^2 < 1$ and $\varpi_o^2 < 1$), while in the domain $\mathfrak{D}_A$ their superior limits are fixed by purely graphical reasons.

From the operational viewpoint, at least two $\boldsymbol{\varpi}$-loci can be recognized to enable the compatible design of metamaterials with extreme spectral behavior. Indeed,

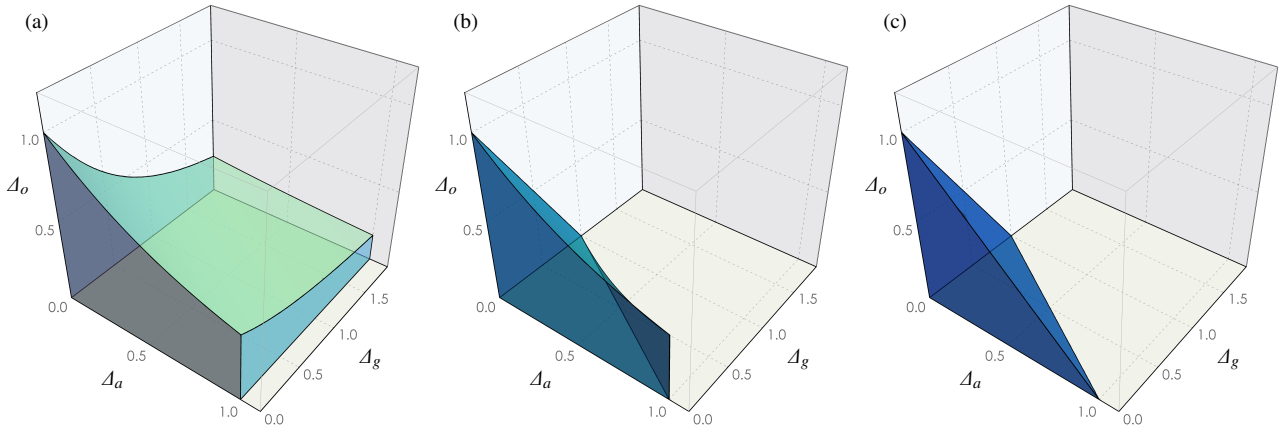

Figure 4: Three-dimensional domains of spectral compatibility in the bandwidth space $\boldsymbol{\Delta} = \{\Delta_a, \Delta_g, \Delta_o\}$: (a) domain $\mathfrak{B}_A$ compatible with *Criterion A*, (b) domain $\mathfrak{B}_B$ compatible with *Criterion B*, (c) domain $\mathfrak{B}_C$ compatible with *Criterion C*.

the boundary $\partial\mathfrak{D}_J$ includes the surfaces $\mathfrak{P}_p$ and $\mathfrak{P}_s$, lying on the planes defined by equations $\varpi_a = \varpi_g$ and $\varpi_o = \varpi_g$. The points $\boldsymbol{\varpi} \in \mathfrak{D}_J$ sitting in the proximity of $\mathfrak{P}_p$ or $\mathfrak{P}_s$ are characterized by relations $\varpi_g - \varpi_a = \epsilon$ or $\varpi_o - \varpi_g = \epsilon$ (with ϵ arbitrarily small) and correspond to *extreme* metamaterials characterized by vanishing stop band (*super-propagators*) or by vanishing optical band (*super-filters*), respectively. Since the surfaces $\mathfrak{P}_p$ or $\mathfrak{P}_s$ bound but not belong to the domain $\mathfrak{D}_J$, perfectly extreme metamaterials with null stop or optical bandwidth are intended to be realizable asymptotically (for $\epsilon \to 0$).

The compatibility domains $\mathfrak{B}_J$ defined within the space of bandwidths $\boldsymbol{\Delta} = \{\Delta_a, \Delta_g, \Delta_o\}$ are represented in Figure 4. The $\boldsymbol{\varpi}$-to-$\boldsymbol{\Delta}$ mapping (21) of the representation space slightly modifies the geometric nature of the domains $\mathfrak{B}_J$, that are three-dimensional simple-connected convex ($\mathfrak{B}_C$) or not convex ($\mathfrak{B}_A$ and $\mathfrak{B}_B$) regions. The boundaries $\partial\mathfrak{B}_J$ are composed by either planar or curved surfaces delimited by straight and curved edges. As minor remark, the domains $\mathfrak{B}_A$ and $\mathfrak{B}_B$ are not convex. From the physical viewpoint, the acoustic and optical bandwidths Δ_a and Δ_o have a superior limit ($\Delta_a < 1$ and $\Delta_o < 1$) for all the domains, whereas the gap bandwidth Δ_g has a superior limit ($\Delta_g < 1$) only for the domains $\mathfrak{B}_B$ and $\mathfrak{B}_C$, while in the domain $\mathfrak{D}_A$ its superior limit is fixed by graphical reasons. The domain representation in the $\boldsymbol{\Delta}$-space allows to appreciate that the largest compatible acoustic and optical bandwidths are identical ($\Delta_a = \Delta_o = 1$). From the operational viewpoint, metamaterials with high filtering performances (namely $\Delta_g > 1$) can be realized only according to Criterion A.

3.3. Iso-transmission band structures

The intersections of the compatibility domains in the space $\mathfrak{W}^2$ generate multi-compatibility domains $\mathfrak{D}_k$ that can be denoted as *mono-compatible* ($k = 1$), *bi-compatible* ($k = 2$) and *three-compatible* ($k = 3$) domains and defined according to the relations

$$\begin{aligned} \mathfrak{D}_3 &= \mathfrak{D}_A \cap \mathfrak{D}_B \cap \mathfrak{D}_C \\ \mathfrak{D}_2 &= \mathfrak{D}_A \cap \mathfrak{D}_B \setminus \mathfrak{D}_3 \\ \mathfrak{D}_1 &= \mathfrak{D}_A \setminus \mathfrak{D}_2 \setminus \mathfrak{D}_3 \end{aligned} \tag{33}$$

The multi-compatible domains are illustrated in the frequency space $\mathfrak{W}^2$ (Figure 5a), and the corresponding multi-compatible domains $\mathfrak{B}_k$ in the bandwidth space $\boldsymbol{\Delta}$ (Figure 5b). Primary attention can be focused on the *three-compatible* domains $\mathfrak{D}_3$ and $\mathfrak{B}_3$ (red regions) that offer the spectral designer the valuable opportunity to design three different inertially amplified metamaterials with *iso-transmission band structures*. As way of example, a point P characterized by the target band structure $\boldsymbol{\varpi}^2_* = (3/10, 5/10, 6/10)$ has been selected and the

Table 1: Mechanical properties of the designed metamaterials.

Design parameters	ϱ^2	η	α
Metamaterial $\mathcal{M}^p_A$	7/3	5/2	$\simeq 27°$
Metamaterial $\mathcal{M}^p_B$	1	1/2	$\simeq 33°$
Metamaterial $\mathcal{M}^p_C$	2/3	3/4	$\simeq 21°$
Metamaterial $\mathcal{M}^p_P$	1/9	9/14	$\simeq 27°$
Metamaterial $\mathcal{M}^p_S$	1	1/8	$\simeq 39°$

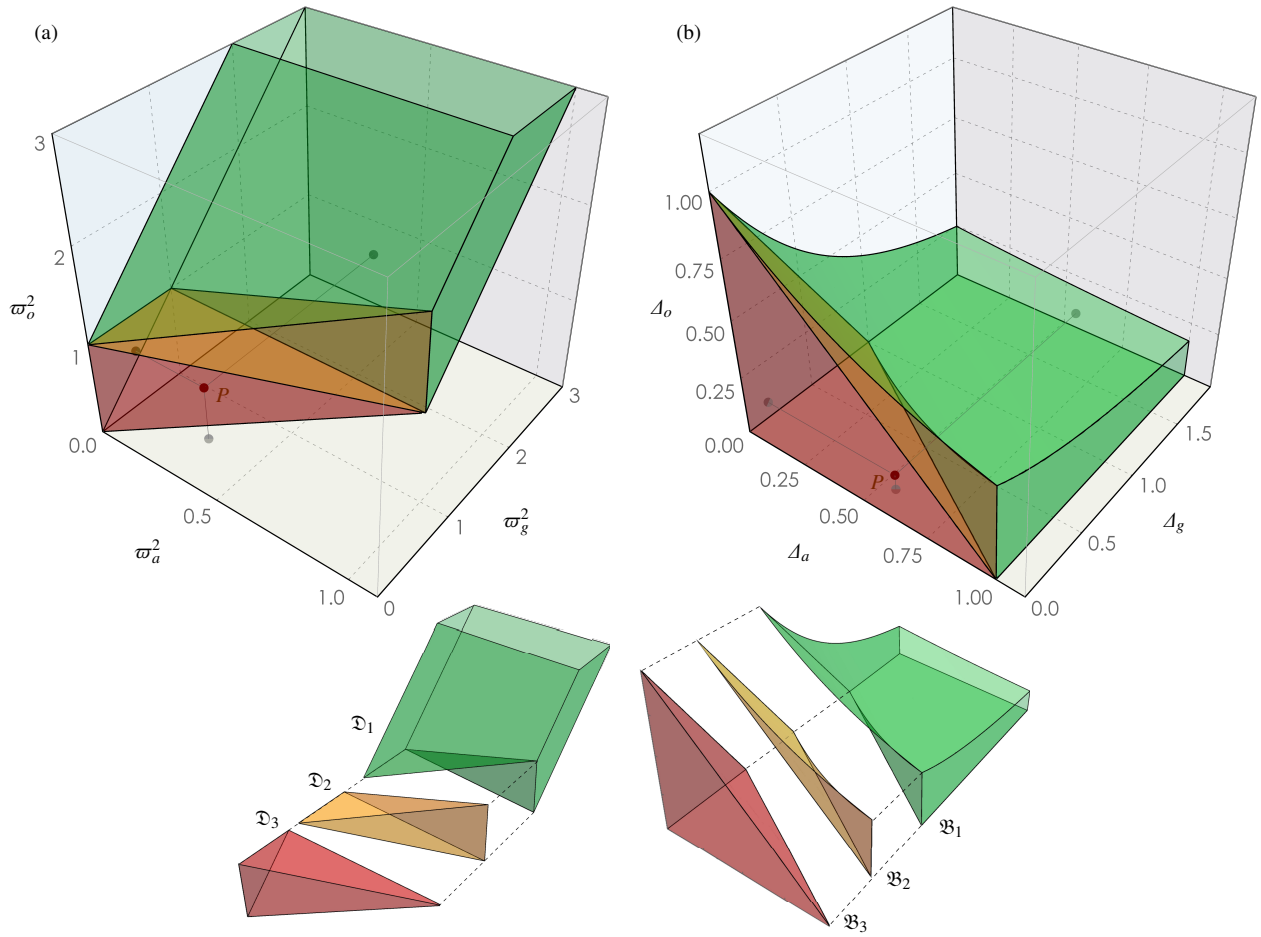

Figure 5: Three-dimensional domains of spectral multi-compatibility: (a) domains $\mathfrak{D}_3$ (red), $\mathfrak{D}_2$ (yellow), $\mathfrak{D}_1$ (green) in the space of (square) spectral bounds $\boldsymbol{\varpi}^2 = \{\varpi_a^2, \varpi_g^2, \varpi_o^2\}$: (b) domains $\mathfrak{B}_3$ (red), $\mathfrak{B}_2$ (yellow), $\mathfrak{B}_1$ (green) in the space of spectral bandwidths $\boldsymbol{\Delta} = \{\Delta_a, \Delta_g, \Delta_o\}$.

corresponding three metamaterials $\mathcal{M}_A^p$, $\mathcal{M}_B^p$, $\mathcal{M}_C^p$ have been designed according to the formulas (26), particularized for the three different criteria. The three sets of mechanical parameters $\mathbf{p}_A = \mathbf{g}_A(\boldsymbol{\varpi}_*^2)$, $\mathbf{p}_B = \mathbf{g}_B(\boldsymbol{\varpi}_*^2)$ and $\mathbf{p}_C = \mathbf{g}_C(\boldsymbol{\varpi}_*^2)$ are reported in Table 1, while the corresponding dispersion properties are are illustrated in Figure 6. Specifically, the frequency dispersion spectra $\mathcal{S}_A$, $\mathcal{S}_B$, $\mathcal{S}_C$ defined by the direct form $\omega(\beta)$ of the dispersion function (18) are reported in Figure 6a. Furthermore, the group velocity spectra $\mathcal{G}_A$, $\mathcal{G}_B$, $\mathcal{G}_C$, defined by the group velocity function $v_g(\beta)$ – determined from the dispersion function (18) according to the expression $v_g(\beta) = \left(\Re(\partial\beta/\partial\omega)\right)^{-1}$ and coincident with the energy velocity [20] – are reported in Figure 6b. As successful verification of the design effectiveness, all the frequency dispersion spectra $\mathcal{S}_A$, $\mathcal{S}_B$, $\mathcal{S}_C$ actually correspond to the target band structure $\boldsymbol{\varpi}_*^2$, although the acoustic and optical branches of the spectra may significantly differ for each metamaterial (Figure 6a). Particularly, metamaterials $\mathcal{M}_A^p$ and $\mathcal{M}_B^p$ show identical frequency and group velocity spectra (i.e. $\mathcal{S}_A = \mathcal{S}_B$ and $\mathcal{G}_A = \mathcal{G}_B$), different from the spectra of metamaterial $\mathcal{M}_C^p$ (i.e. $\mathcal{S}_A \neq \mathcal{S}_C$ and $\mathcal{G}_A \neq \mathcal{G}_C$). Nonetheless, this occurrence cannot be considered a systematic finding, because iso-band structured infinite metamaterials do not result from the specific search of isospectral or quasi isospectral finite systems, as commonly intended in the literature [40–43]. Furthermore, it can be remarked that – for a fixed wavenumber β – the isofrequency complex-valued waveforms (acoustic $\boldsymbol{\varphi}_J^-$ and optical $\boldsymbol{\varphi}_J^+$) of the metamaterials $\mathcal{M}_A^p$ and $\mathcal{M}_B^p$ generally differ. Such waveform difference determines dissimilar wave polarizations (see the real form of the waveforms in Figure 6a), without anyway compromising the identity between the group and energy velocities, as expected. As complementary remark, it is worth noting

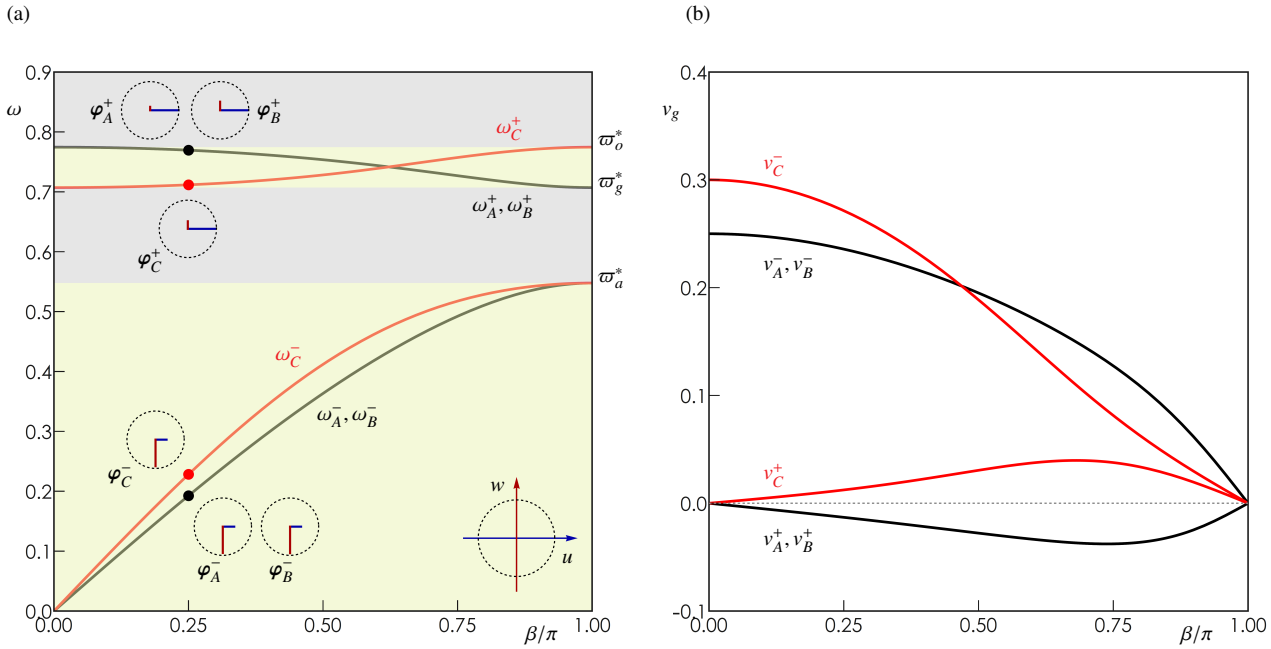

Figure 6: Dispersion spectra of the designed metamaterials $\mathcal{M}_A^p$, $\mathcal{M}_B^p$, $\mathcal{M}_C^p$: (a) frequency spectra $\mathcal{S}_A$, $\mathcal{S}_B$ (black dispersion curves), $\mathcal{S}_C$ (red dispersion curves) with real forms of the complex-valued waveforms at wavenumber $\beta = \pi/4$; (b) group velocity spectra $\mathcal{G}_A$, $\mathcal{G}_B$ (black dispersion curves), $\mathcal{G}_C$ (red dispersion curves).

that differences in the waveforms can also determine different spectral behaviors in the nonlinear regime of high-amplitude oscillations [33], like for instance different nonlinear frequencies associated to metamaterials with the same linear frequency spectrum.

From the viewpoint of microstructural design, it can be remarked that the same spectral target $\boldsymbol{\varpi}_*^2$ is achievable by realizing metamaterials with significantly different set $\mathbf{p}$ of physical properties. Indeed, if the nondimensional parameters ϱ^2, η and α are mechanically interpreted as indices of the metamaterial mass, deformability and thickness, respectively, the designed metamaterials are characterized by

- $\mathcal{M}_A^p$: low deformability, high mass, middle thickness
- $\mathcal{M}_B^p$: high deformability, middle mass, large thickness
- $\mathcal{M}_C^p$: middle deformability, low mass, small thickness

Accordingly, one or the other design solution can be preferred for extra functionalization, that is to exalt the static properties of lightness, stiffness or slenderness. Alternately, other dynamic properties can be customized, for instance by targeting an optimal government of the elastic energy flows. Indeed, metamaterial $\mathcal{M}_C^p$ can be preferred to maximize the group and energy velocity of the acoustic waves propagating in the range of long wavelengths, or metamaterials $\mathcal{M}_A^p$ and $\mathcal{M}_B^p$ can be chosen to achieve negative group and energy velocities of the optical waves (see Figure 6b).

3.4. *Superpropagators and superfilters*

Focusing on the extreme spectral design, minimizing the stop bandwidth or the optical bandwidth can be a target of theoretical and technological interest, with the aim of realizing superpropagating or superfiltering devices. To this purpose, imposing the limit condition of null stop bandwidth ($\boldsymbol{\varpi}_*^2 \in \mathfrak{P}_p$) makes the associations $\mathfrak{a}_A(\omega^2)$ and $\mathfrak{a}_B(\omega^2)$ in equation (25) coincident to each other (identity of Criteria A and B). Furthermore, recalling the physical inequality $\omega_3^2(\mathbf{p}) > \omega_2^2(\mathbf{p})$, null stop bandwidth cannot be obtained following Criterion C. Similarly, imposing the limit condition of null optical bandwidth ($\boldsymbol{\varpi}_*^2 \in \mathfrak{P}_s$) makes the associations $\mathfrak{a}_B(\omega^2)$ and $\mathfrak{a}_C(\omega^2)$ coincident to each other (identity of Criteria B and C). Moreover, the physical inequality $\omega_3^2(\mathbf{p}) > \omega_2^2(\mathbf{p})$ states that null optical bandwidth cannot be obtained following Criterion A.

Based on these considerations, two metamaterials with extreme spectral behavior have been designed by selecting a particular couple of points P_P and P_S belonging to the surfaces $\mathfrak{P}_p$ and $\mathfrak{P}_s$, respectively. Points P_P and P_S are shown in Figure 7a, illustrating surfaces $\mathfrak{P}_p$ and $\mathfrak{P}_s$ in the three-dimensional space $\mathfrak{W}^2$ of band structures. Specifically, the band structure of the two points asymptotically satisfies the conditions $\varpi_{ag}^* = \varpi_g^* = \varpi_a^*$ and $\varpi_{go}^* = \varpi_g^* = \varpi_o^*$, respectively (particularly, the target band structures $\boldsymbol{\varpi}_*^2 = (9/10, 9/10, 16/10)$ and $\boldsymbol{\varpi}_*^2 = (1/10, 5/10, 5/10)$ have been selected for P_P and

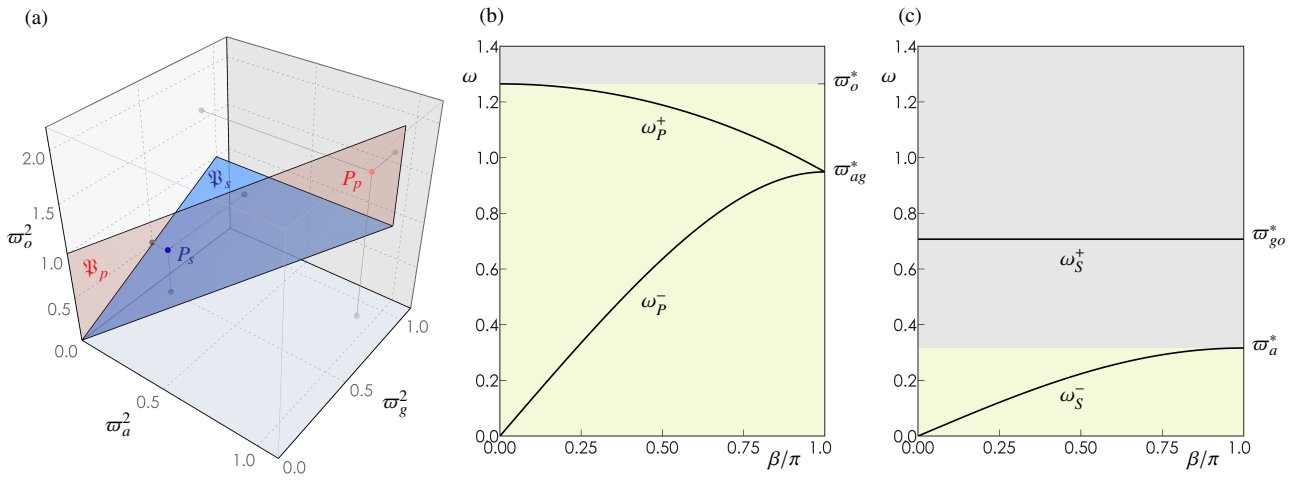

Figure 7: Design of extreme metamaterials: (a) compatible surfaces $\mathfrak{P}_p$ (red) and $\mathfrak{P}_s$ (blue) in the three-dimensional space $\mathfrak{W}^2$ of band structures; (b) dispersion spectrum of the superpropagator $\mathcal{M}_P^p$ (red point P_p on $\mathfrak{P}_p$), (b) dispersion spectrum of the superfilter $\mathcal{M}_S^p$ (blue point P_s on $\mathfrak{P}_s$).

P_S, respectively). Consequently, the extreme metamaterials are characterized by vanishing stop bandwidth (superpropagator $\mathcal{M}_P^p$) and vanishing optical bandwidth (superfilter $\mathcal{M}_S^p$). The respective sets of mechanical parameters $\mathbf{p}_P$ (determined according to Criterion A or B) and $\mathbf{p}_S$ (determined according to Criterion B or C) are reported in Table 1. The associated dispersion spectra, characterized by two spectral bands, are portrayed in Figures 7b,c. The correctness of the extreme design is successfully verified for both the superpropagator $\mathcal{M}_P^p$, exhibiting a two-band pass-pass structure (Figures 7b), and for the superfilter $\mathcal{M}_S^p$, exhibiting a two-band pass-stop structure (Figures 7c). As final remark, it can be noted that the mechanical parameters of the extreme metamaterials do not stand at the extremes of the admissible parameter ranges. Thus, superpropagators and superfilters can be realized without extremizing the design parameters.

Conclusions

A one-dimensional periodic lattice is considered as minimal physical realization of a non-dissipative mechanical metamaterial with pantographic inertia amplification. The tetra-atomic composite microstructure of the repetitive elementary cell is characterized by two principal point masses, aligned along the metamaterial axis and elastically interconnected, that are pantographically coupled with a pair of eccentric secondary point masses, serving as local inertial amplifiers. By virtue of the axial indeformability of the pantograph arms, the undamped free dynamics of the cell is governed by a condensed two-degrees-of-freedom model in the Lagrangian coordinates expressing the axis-aligned displacements of the principal masses. The linearized model is mechanically described by a low-dimension set of three independent nondimensional parameters (mass ratio, stiffness ratio, amplification angle).

First, the free propagation of harmonic waves is parametrically investigated by analytically solving the direct eigenproblem of the uni-modular frequency-dependent transfer matrix. The complex-valued eigenvalues play the role of wavenumber-dependent Floquet multipliers and define the propagation (pass) or attenuation (stop) bands of the dispersion spectrum. The spectral triband structure (pass-stop-pass) is systematically characterized by a low-frequency acoustic branch and a high-frequency optical branch, separated by a band gap. The band-separating frequencies are conveniently expressed as analytical, wavenumber-independent functions (*bounding functions*) in the parameter space. In this respect, it must be noted that the three bounding functions are not univocally sortable in the same ascending order over the entire parameter space.

Second, the spectral design is approached according to a general strategy consisting in stating an inverse eigenproblem, in which a certain band structure is imposed as known input, while the parameter set realizing the corresponding band-structured metamaterial is the unknown output. Due to the inherent nonlinearity of the inverse problem, existence and uniqueness of the solution in the admissible ranges of the parameter space have to be discussed. For the pantographic metamaterial, the valuable possibility of inverting analytically the bounding functions (analytical spectral design) allows demonstrating the existence and unique-

ness of the solution. Nonetheless, the different possible orders of the bounding functions in different regions of the parameter space offer a multiplicity of solution schemes for the inverse problem. Disregarding the orders that do not satisfy physical consistency, only three admissible solution schemes, or *design criteria*, can be adopted. Each design criterion provides explicit formulas for the three mechanical parameters (output) realizing the target band structure (input). Eventually, the admissible ranges of the mechanical parameters are combined with the design formulas to obtain the compatibility domains collecting all the band structures physically realizable according to each criterion. As interesting finding, multi-compatible domains corresponding to band structures realizable by different metamaterials (iso-band structured metamaterials), designed according to different criteria, are obtained.

Finally, the design formulas are effectively applied to identify iso-band structured metamaterials, characterized by different stiffnesses, inertias and geometries. This achievement paves the way for developing entire functional classes of inertially amplified metamaterials featuring the same spectral performances, but different flexibility and/or lightness. In this respect, it is worth remarking that the analytical spectral design is naturally robust, meaning that – in general – its application does not suffer for the common well-posedness or convergence issues that may negatively affect other design and optimization problems related to material and metamaterial functionalization. As valuable completion, pantographic metamaterials with extreme spectral properties – including vanishing stop bandwidth or vanishing optical bandwidth – are successfully designed.

As concluding consideration, the general strategy based on formulating the spectral design as an analytically solvable inverse eigenproblem is rather flexible and adaptable to different design targets and/or other composite microstructures with complex topologies. In this respect – if necessary – the strategy can be developed to include different or additional dispersion properties as design targets, like for instance lower or higher group velocities for the acoustic or optical waves propagating within a certain range of wavelengths.

Acknowledgments

The authors gratefully acknowledge financial support from National Group of Mathematical Physics (GNFM-INdAM), from the Compagnia San Paolo, project MINIERA no. I34I20000380007 and from University of Trento, project UNMASKED 2020.

References

[1] Bonnet M., Constantinescu A. (2005). Inverse problems in elasticity. *Inverse problems*, 21(2):R1–R50.

[2] Gladwell G. M., Morassi A. (2011). *Dynamical inverse problems: theory and application*, volume 529. Springer Science & Business Media.

[3] Marchenko V., Slavin V. (2018). *Inverse problems in the theory of small oscillations*, volume 247. American Mathematical Soc.

[4] Krushynska A., Kouznetsova V., Geers M. (2014). Towards optimal design of locally resonant acoustic metamaterials. *Journal of the Mechanics and Physics of Solids*, 71:179–196.

[5] Lepidi M., Bacigalupo A. (2018). Parametric design of the band structure for lattice materials. *Meccanica*, 53(3):613–628.

[6] Vadalà F., Bacigalupo A., Lepidi M., Gambarotta L. (2018). Bloch wave filtering in tetrachiral materials via mechanical tuning. *Composite Structures*, 201:340–351.

[7] Bacigalupo A., De Bellis M. L., Misseroni D. (2020). Design of tunable acoustic metamaterials with periodic piezoelectric microstructure. *Extreme Mechanics Letters*, 40:100977.

[8] Diaz A., Haddow A., Ma L. (2005). Design of band-gap grid structures. *Structural and Multidisciplinary Optimization*, 29(6):418–431.

[9] Li W., Meng F., Chen Y., Li Y. F., Huang X. (2019). Topology optimization of photonic and phononic crystals and metamaterials: A review. *Advanced Theory and Simulations*, 2(7):1900017.

[10] Bruggi M., Corigliano A. (2019). Optimal 2d auxetic microstructures with band gap. *Meccanica*, 54(13):2001–2027.

[11] Ronellenfitsch H., Stoop N., Yu J., Forrow A., Dunkel J. (2019). Inverse design of discrete mechanical metamaterials. *Physical Review Materials*, 3(9):095201.

[12] Roca D., Yago D., Cante J., Lloberas-Valls O., Oliver J. (2019). Computational design of locally resonant acoustic metamaterials. *Computer Methods in Applied Mechanics and Engineering*, 345:161–182.

[13] Goh H., Kallivokas L. F. (2019). Inverse metamaterial design for controlling band gaps in scalar wave problems. *Wave Motion*, 88:85–105.

[14] Wu L., Liu L., Wang Y., Zhai Z., Zhuang H., Krishnaraju D., Wang Q., Jiang H. (2020). A machine learning-based method to design modular metamaterials. *Extreme Mechanics Letters*, 36:100657.

[15] Bacigalupo A., Gnecco G., Lepidi M., Gambarotta L. (2020). Machine-learning techniques for the optimal design of acoustic metamaterials. *Journal of Optimization Theory and Applications*, 187(3):630–653.

[16] Bacigalupo A., Gnecco G., Lepidi M., Gambarotta L. (2021). Computational design of innovative mechanical metafilters via adaptive surrogate-based optimization. *Computer Methods in Applied Mechanics and Engineering*, 375:113623.

[17] Colquitt D. J., Brun M., Gei M., Movchan A. B., Movchan N. V., Jones I. S. (2014). Transformation elastodynamics and cloaking for flexural waves. *Journal of the Mechanics and Physics of Solids*, 72:131–143.

[18] Yang M., Sheng P. (2017). Sound absorption structures: From porous media to acoustic metamaterials. *Annual Review of Materials Research*, 47:83–114.

[19] Billon K., Zampetakis I., Scarpa F., Ouisse M., Sadoulet-Reboul E., Collet M., Perriman A., Hetherington A. (2017). Mechanics and band gaps in hierarchical auxetic rectangular perforated

composite metamaterials. *Composite Structures*, 160:1042–1050.

[20] Bacigalupo A., Lepidi M. (2018). Acoustic wave polarization and energy flow in periodic beam lattice materials. *International Journal of Solids and Structures*, 147:183–203.

[21] D'Alessandro L., Ardito R., Braghin F., Corigliano A. (2019). Low frequency 3D ultra-wide vibration attenuation via elastic metamaterial. *Scientific Reports*, 9(1):8039.

[22] Bordiga G., Cabras L., Bigoni D., Piccolroaz A. (2019). Free and forced wave propagation in a Rayleigh beam grid: flat bands, Dirac cones, and vibration localization vs isotropization. *International Journal of Solids and Structures*, 161:64–81.

[23] Ma T.-X., Fan Q.-S., Li Z.-Y., Zhang C., Wang Y.-S. (2020). Flexural wave energy harvesting by multi-mode elastic metamaterial cavities. *Extreme Mechanics Letters*, 41:101073.

[24] Pechac J. E., Frazier M. J. (2022). Metamaterial design strategy for mechanical energy absorption under general loading. *Extreme Mechanics Letters*, 51:101580.

[25] Gao Y., Wang L. (2022). Active multifunctional composite metamaterials with negative effective mass density and negative effective modulus. *Composite Structures*, 291:115586.

[26] Yilmaz C., Hulbert G. (2010). Theory of phononic gaps induced by inertial amplification in finite structures. *Physics Letters A*, 374(34):3576–3584.

[27] Bilal O. R., Hussein M. I. (2013). Trampoline metamaterial: Local resonance enhancement by springboards. *Applied Physics Letters*, 103(11):111901.

[28] Ma G., Sheng P. (2016). Acoustic metamaterials: From local resonances to broad horizons. *Science advances*, 2(2):e1501595.

[29] Meaud J., Che K. (2017). Tuning elastic wave propagation in multistable architected materials. *International Journal of Solids and Structures*, 122:69–80.

[30] Yilmaz C., Hulbert G. M., Kikuchi N. (2007). Phononic band gaps induced by inertial amplification in periodic media. *Physical Review B*, 76(5):054309.

[31] Barys M., Jensen J. S., Frandsen N. M. (2018). Efficient attenuation of beam vibrations by inertial amplification. *European Journal of Mechanics-A/Solids*, 71:245–257.

[32] Muhammad S., Wang S., Li F., Zhang C. (2020). Bandgap enhancement of periodic nonuniform metamaterial beams with inertial amplification mechanisms. *Journal of Vibration and Control*, 26(15–16):1309–1318.

[33] Settimi V., Lepidi M., Bacigalupo A. (2021). Nonlinear dispersion properties of one-dimensional mechanical metamaterials with inertia amplification. *International Journal of Mechanical Sciences*, 201:106461.

[34] Yuksel O., Yilmaz C. (2020). Realization of an ultrawide stop band in a 2-d elastic metamaterial with topologically optimized inertial amplification mechanisms. *International Journal of Solids and Structures*, 203:138–150.

[35] Frandsen N. M., Bilal O. R., Jensen J. S., Hussein M. I. (2016). Inertial amplification of continuous structures: Large band gaps from small masses. *Journal of Applied Physics*, 119(12):124902.

[36] Banerjee A., Adhikari S., Hussein M. I. (2021). Inertial amplification band-gap generation by coupling a levered mass with a locally resonant mass. *International Journal of Mechanical Sciences*, 207:106630.

[37] Hennig D., Tsironis G. P. (1999). Wave transmission in nonlinear lattices. *Physics Reports*, 307(5-6):333–432.

[38] Romeo F., Luongo A. (2002). Invariant representation of propagation properties for bi-coupled periodic structures. *Journal of Sound and Vibration*, 257(5):869–886.

[39] Bronski J. C., Rapti Z. (2005). Modulational instability for nonlinear Schrödinger equations with a periodic potential. *Dynamics of Partial Differential Equations*, 2(4):335–355.

[40] Gladwell G., Morassi A. (1995). On isospectral rods, horns and strings. *Inverse Problems*, 11(3):533–555.

[41] Gladwell G. (1995). On isospectral spring-mass systems. *Inverse Problems*, 11(3):591–602.

[42] Gottlieb H. (2002). Isospectral strings. *Inverse Problems*, 18(4):971–987.

[43] Lepidi M. (2013). Multi-parameter perturbation methods for the eigensolution sensitivity analysis of nearly-resonant non-defective multi-degree-of-freedom systems. *Journal of Sound and Vibration*, 332(4):1011–1032.